Received: 30 August 2022 | Revised: 25 November 2022 | Accepted: 2 December 2022

DOI: 10.1002/btpr.3318

BIOTECHNOLOGY PROGRESS

RESEARCH ARTICLE

Cell Culture and Tissue Engineering

Real-time online monitoring of insect cell proliferation and baculovirus infection using digital differential holographic microscopy and machine learning

Jort J. Altenburg[1] | Maarten Klaverdijk[1] | Damien Cabosart[2] | Laurent Desmecht[2] | Sonja S. Brunekreeft-Terlouw[1] | Joshua Both[1] | Vivian I. P. Tegelbeckers[1] | Marieke L. P. M. Willekens[1] | Linda van Oosten[3] | Tessy A. H. Hick[1,3] | Tom M. H. van der Aalst[1] | Gorben P. Pijlman[3] | Monique M. van Oers[3] | René H. Wijffels[1] | Dirk E. Martens[1]

[1]Bioprocess Engineering, Wageningen University & Research, Wageningen, The Netherlands

[2]Ovizio Imaging Systems, Ukkel, Belgium

[3]Laboratory of Virology, Wageningen University & Research, Wageningen, The Netherlands

Correspondence
Jort J. Altenburg, Department of Bioprocess Engineering, Wageningen University & Research, Droevendaalsesteeg 1, 6708 PB Wageningen, The Netherlands.
Email: jort.altenburg@wur.nl

Funding information
NWO Domain Applied and Engineering Sciences, Grant/Award Number: 16726

Abstract

Real-time, detailed online information on cell cultures is essential for understanding modern biopharmaceutical production processes. The determination of key parameters, such as cell density and viability, is usually based on the offline sampling of bioreactors. Gathering offline samples is invasive, has a low time resolution, and risks altering or contaminating the production process. In contrast, measuring process parameters online provides more safety for the process, has a high time resolution, and thus can aid in timely process control actions. We used online double differential digital holographic microscopy (D3HM) and machine learning to perform non-invasive online cell concentration and viability monitoring of insect cell cultures in bioreactors. The performance of D3HM and the machine learning model was tested for a selected variety of baculovirus constructs, products, and multiplicities of infection (MOI). The results show that with online holographic microscopy insect cell proliferation and baculovirus infection can be monitored effectively in real time with high resolution for a broad range of process parameters and baculovirus constructs. The high-resolution data generated by D3HM showed the exact moment of peak cell densities and temporary events caused by feeding. Furthermore, D3HM allowed us to obtain information on the state of the cell culture at the individual cell level. Combining this detailed, real-time information about cell cultures with methodical machine learning models can increase process understanding, aid in decision-making, and allow for timely process control actions during bioreactor production of recombinant proteins.

KEYWORDS

bioengineering, biotechnology, cell culture, process sensing and control

1 | INTRODUCTION

The baculovirus-insect cell expression vector system (BEVS) is used for the production of recombinant proteins and is one of the most used eukaryotic expression platforms to produce virus-like particles (VLPs).[1–4] With this expression platform, VLP quantities comparable to those achieved in yeast can be produced. In addition, with BEVS it is possible to perform post-translational modifications (PTMs), such as glycosylation, comparable (but not identical) to that of mammalian cells.[5–7] The baculovirus vector constructs required for the expression of the desired proteins (e.g., VLPs, viral glycoproteins, gene therapy vectors, enzymes, and biologicals) can be generated in a matter of weeks. The ability to quickly express the desired protein and scale up the production makes the BEVS an excellent platform to respond to emerging virus threats, as witnessed recently during the global COVID-19 pandemic and earlier during outbreaks of the Zika virus.[8–10]

When scaling up the BEVS in bioreactors, it is important to determine three key parameters that interact with each other; the cell density at infection (CCI), multiplicity of infection (MOI), and the optimal time of harvest (TOH). First, cells are grown to the CCI at which point the baculovirus particles are added at a certain MOI, that is, number of infectious virus particles per viable cell. Approximately 20–24 h after the insect cells are infected by the baculoviruses they start producing the protein of interest. Next, at approximately 48–72 h after infection, the cells start to lyse and release their contents in the medium among which proteases. This may affect product quality and complicate downstream processing, essentially lowering the product yield. On the other hand, performing the harvest too early leads to reduced yields as well. Harvesting at the right TOH is therefore critical for obtaining optimal yields of a high-quality product. Being able to precisely determine the values for CCI, MOI, and TOH during process development is essential for obtaining optimal volumetric productivity and product quality in the final production process.

Key process parameters describing the state of the culture, like viable cell density, viability, and infection state of the culture, are usually measured only once or twice per day. As a result, the time resolution (once every 12–24 h) is low and important information to determine for example cell growth or infection stage may be obtained too late or even completely missed. This leads to suboptimal control and potential failure of production runs.[11] In addition, insufficient information is obtained for a proper mechanistic understanding of the system. For example, when developing mathematical models based on scattered, offline sample data, the low time resolution of the data will impact the quality of these models. Finally, such manual sampling also introduces the risk of contaminating the culture and is prone to operator variance leading to less reliable datasets. Thus, online and real-time measurement of key parameters like viable cell density, viability, and infection state of the culture appears to be important for a proper understanding of the BEVS and timely control of the production process.

Currently, several physical probes are available to allow online measurements of biomass, such as dielectric spectroscopy and light scattering. Dielectric spectroscopy measures viable biomass based on biomass capacitance, whereas light scattering methods measure total biomass.[12–14] These methods are well suited for measuring cell biomass, however, they cannot directly measure the viability or infection stage of a single cell. Image-based cell culture monitoring is a more direct approach, where cells can be visualized individually to extract both the cell density and information on the state of the cells. An example of such an online imaging tool is online double digital differential holographic microscopy (D3HM).[15,16] With this technique, the cell density is measured as well as a large number of optical parameters among which cell diameter and circularity, as well as quantitative parameters associated with the light phase and light intensity of each cell. These parameters can be related to the physiological states of the cells using machine learning models and specific training data sets. There is currently only one study that demonstrated the ability of online double digital differential holographic microscopy to monitor the BEVS in bioreactors.[17] In that study by Pais et al. (2020), two bioreactor batch runs of Sf9 cells in SF900 II medium were performed where the insect cell concentration was measured online and the viability and AAV production titer was predicted. One growth batch without baculovirus infection and a single AAV production run using a two-baculovirus infection strategy at an MOI of 0.05 $TCID_{50}$/cell were monitored.

The current work aims to obtain more insight into the performance of online digital differential holographic microscopy to monitor baculovirus-infected cell cultures in bioreactors. Several baculovirus constructs were included, producing various recombinant proteins, and under varying process conditions, using the ExpiSf9 cell line as a model.[18] First, training data sets were generated to develop machine learning models. Then the performance of the D3HM tool and machine learning model was evaluated during online monitoring of bioreactor runs. Results showed that after training the machine algorithm with a training data set, the cell density, cell viability, cell diameter, and the fraction of infected cells could be accurately determined for a variety of bioreactor processes. Furthermore, the continuous online measurements allowed for the construction of high-resolution time-series profiles of these parameters. These high-resolution time-series profiles gave more insight into the state of the cell culture inside the bioreactor. Infected cells could be detected earlier compared to offline methods and the effect of process interventions such as feeding became distinguishable. Improved training data sets can further increase the accuracy of the online prediction, allowing for more advanced process control strategies and increased process understanding of recombinant protein production processes.

2 | MATERIALS AND METHODS

2.1 | Cell lines, media, and virus stocks

ExpiSf9 cells (Thermo Fisher) adapted to ExpiSf chemically defined medium (Thermo Fisher) were used in all batch and shake flask cultures. Recombinant baculoviruses of Autographa californica

multicapsid nucleopolyhedrovirus (AcMNPV) were generated in two ways. Baculovirus expressing His-tagged GFP (hisGFP) or mCherry from the polyhedrin promoter, and a dual fluorescence baculovirus (AcBac-2FL) with GFP driven by the OpMNPV IE2 promoter and mCherry from the polyhedrin promoter were constructed by bac-to-bac transposition in *Escherichia coli* (Thermo Fisher), followed by transfection of the bacmid into Sf9 insect cells with Expres2TR transfection reagent (Expres2ion Biotechnologies). Baculovirus expressing the strep-tagged SARS-COV-2 S1 spike subunit from the polyhedrin promoter was constructed by using pOET1-derived plasmids to transfect insect cells with the flashBAC Ultra kit (Oxford Expression Technologies, van Oosten et al., 2021). All baculovirus stocks were amplified in ExpiSf9 cells, and viral titers were determined by endpoint dilution assay on Sf9-easy titer cells using the Reed-Muench method.[19] Viral titers are defined as 50% tissue culture infectious dose ($TCID_{50}$) units per ml.

2.2 | Bioreactor cultures

Cells were grown in 0.5 L miniBio or 3 L glass reactor vessels (Getinge) controlled by myControl bioreactor controllers (Getinge). The working volume of each reactor vessel was 0.3–2 L. Reactors were inoculated at target starting densities of 0.5–1.0 $\times$ 10^6 viable cells/ml. The liquid temperature was controlled at 27°C. The pH was not controlled but maintained by the buffering capacity of the medium. Measured values remained between pH 5.7–6.1. Dissolved oxygen was controlled at 30% of air saturation using Lumisens optical dissolved oxygen sensors (Getinge) and sparging of pure oxygen through open pipe spargers. In addition, a constant headspace aeration rate of 0.01 vvm air was applied. Agitation with marine impellers was set to 266–600 rpm by keeping the tip speed constant among the different reactor sizes.

2.3 | Analytical methods

Cells were counted by trypan blue exclusion using a TC20 Automated Cell Counter (Bio-Rad) or by manual counting using DHC-F01 cell counting chambers (INCYTO). Online measurements of viable and total cell density, viability, and infected cells were performed by differential digital holographic microscopy (D3HM) using iLine F holographic microscopes (OVIZIO). Data acquisition and quantitative data analysis were performed using OsOne software (OVIZIO). Infected cells were visualized by expression of GFP or mCherry detected by a C6 Plus Flow Cytometer (BD Accuri). SARS-CoV-2 S1 subunits were quantified using a SARS-COV-2 Spike S1 Protein ELISA kit (AssayGenie).

3 | RESULTS AND DISCUSSION

3.1 | Training of the machine learning model

We assessed the ability of the iLine F online microscope to monitor cell growth, viability, and virus infection in bioreactors. Cell culture fluid was continuously pumped from the reactor through the iLine F flow cell and back into the reactor again. In this flow cell, holograms of the cells were captured. These holographic pictures allowed for direct calculation of the cell concentration and analysis of a large set of optical cell parameters that can be linked to the state of the cell. For example, upon baculovirus infection, distinct changes in cell morphology occur such as cell enlargement and changes in the granularity of the cell.[20–23] Specific optical changes also occur if the cell loses viability. Changes in measured optical parameters were then linked to the infection state and viability of each separate cell by a machine-learning model (Figure 1). The model was trained by monitoring bioreactor cultures of baculovirus-infected ExpiSf9 suspension cells in ExpiSf chemically defined medium. The training was done for the parameters of viability and infection percentage. Data from 6 runs with around 7 captures per run were used to train the initial machine learning model. To calculate the cell concentration, a segmentation model was used to detect the objects on the images. The objects were then filtered to remove non-cell objects like cell debris by specifying criteria such as particle size. Since the segmentation algorithm was not a machine learning model, no training step was required but only model parameter tuning. Part of the training was a bioreactor run with ExpiSf9 cells that were infected with a baculovirus expressing two fluorescent protein genes at high MOI (3 $TCID_{50}$/cell) (Figure 2). The training data set for the live and dead cell detection algorithm was calibrated using offline samples and standard manual hemocytometer cell counting techniques using trypan blue exclusion. Viable cell percentages were very similar for the online measurement and offline samples except for 96 hours post-inoculation (hpi) when offline measured viability was notably higher (Figure 2a). The machine learning model might have detected dead or dying cells before this was discernable by trypan blue exclusion.

The infected cell detection algorithm was calibrated to offline data from the same baculovirus-infected bioreactor cultures of Expisf9 cells in ExpiSf chemically defined medium. To calibrate the algorithm, a purpose-built dual fluorescence baculovirus construct was engineered. This dual fluorescence baculovirus, AcBac-2FL, was constructed to express the GFP gene behind the immediate early OpIE2 promoter, and the mCherry gene behind the very late polyhedrin promoter. The expression of GFP behind the OpIE2 promoter allowed us to spot early infection as the OpIE2 promoter becomes active immediately after baculovirus infection.[24,25] The expression of mCherry was regulated by the very late polyhedrin promoter commonly used in the BEVS. This polyhedrin promoter becomes active around 20–24 h after baculovirus infection.[26] To generate the training data set, the bioreactor culture was infected with AcBac-2FL at an MOI of 3 $TCID_{50}$/cell. The early and very late phases of baculovirus infection could clearly be distinguished since cells showing green fluorescence were detected 1 day before the appearance of red fluorescent cells (Figure 2b). Using the early expression of GFP in insect cells, the machine learning model for the detection of infected insect cells was then calibrated to offline samples measuring the percentage of green fluorescent cells with a flow cytometer. The iLine F detected the percentage of infected cells before mCherry was detected by the

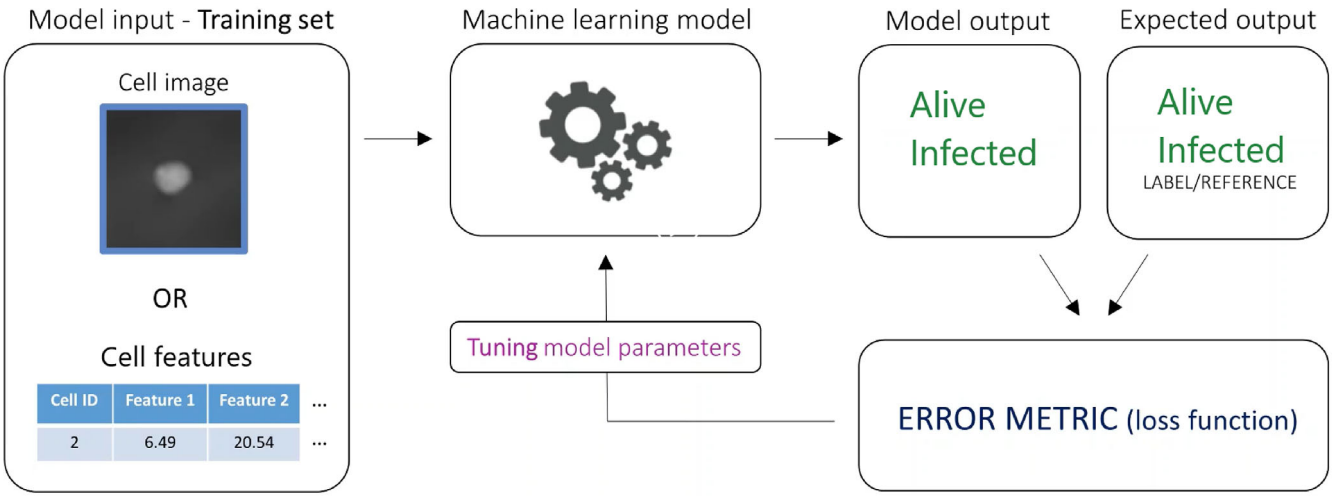

FIGURE 1 Workflow for training the machine learning model to detect alive and dead cells

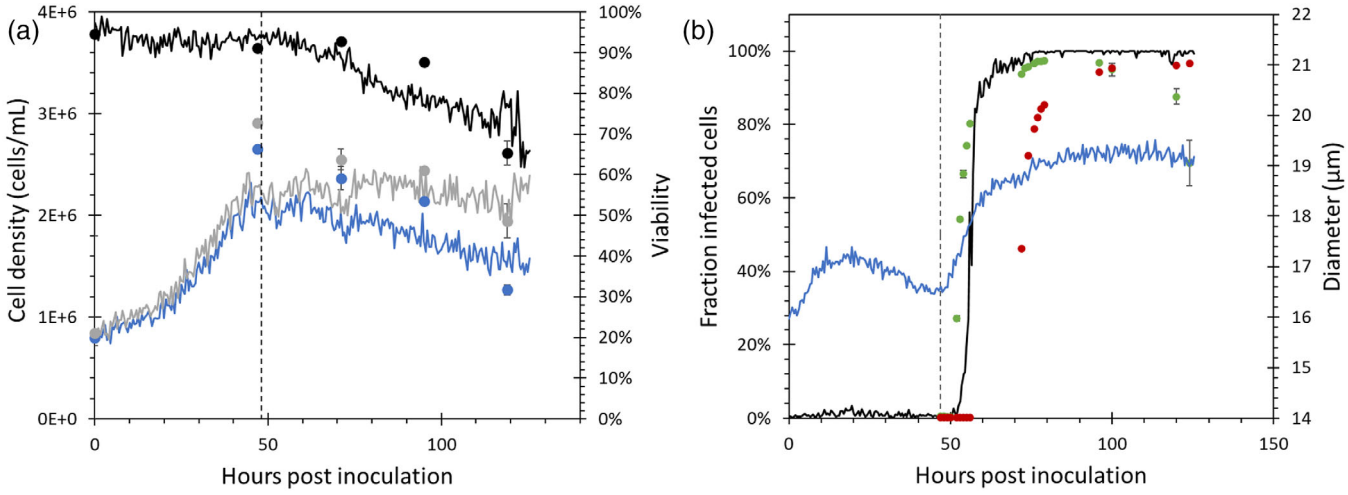

FIGURE 2 Time-course profiles for a training bioreactor run where ExpiSf9 cells were infected with a baculovirus expressing GFP and mCherry at an MOI of 3. The used baculovirus construct, AcBac-2FL, contained a gene for GFP located behind the immediate early OpIE2 promoter and a mCherry gene located behind the very late polyhedrin promoter. The dashed lines indicate the moment of baculovirus infection. (a) Viable online (-) and offline (●) and total online (-) and offline (●) cell densities. Online (-) and offline (●) viable cell percentages. (b) Online predicted infected cell fraction (-), offline measurements of fraction of GFP (●) and mCherry (●) expressing cells and average online cell diameter (-). Error bars represent duplicate measurement values

flow cytometer (about 16 h). However, detection of infection by the iLine F was still slightly delayed (about 4 h) compared to the percentage of infection as determined by immediate early expression of eGFP manually. The eGFP was detected by flowcytometry about 5 h after infection of the culture. This indicated that the expression of early genes preceded detection of optical changes to the cells by the microscope and the machine learning algorithm.

3.2 | Verification run of baculovirus infection at low MOI

After the machine learning model was trained using this training data set, the model was tested using new verification data sets. ExpiSf9 cells were infected with AcBac-2FL at an MOI of 0.01 at a CCI of 1.1×10^6 cells/ml. The bioreactor culture was monitored by the iLine F holographic microscope (Figure 3). Using a low MOI of 0.01 would lead to multiple infection cycles before the complete culture would be infected with baculovirus.

Although online measurements showed a similar trend in measured viable cell density and total cell density compared to offline measurements, both viable and total cell densities were higher for the online measurements (Figure 3a). Since the cell counts are based on image analysis of the flow cell with a known volume and are extensively verified by the supplier, it might be that the difference is caused by the loss of cells during the offline sample handling. When taking samples offline and measuring them manually with the iLine F, cell counts were more similar between hemocytometer and holographic

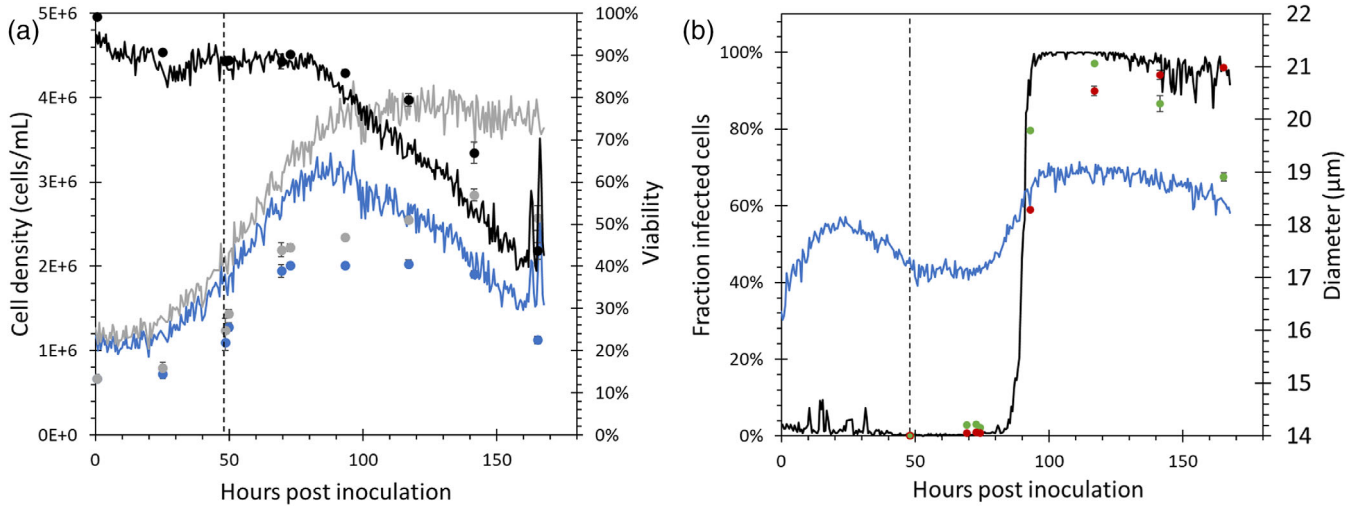

FIGURE 3 Time-course profiles for a verification bioreactor run where ExpiSf9 cells were infected with a baculovirus expressing GFP and mCherry at an MOI of 0.01. The used baculovirus construct, AcBac-2FL, contained a gene for GFP located behind the immediate early OpIE2 promoter and a mCherry gene located behind the very late polyhedrin promoter. The dashed lines indicate the moment of baculovirus infection. (a) Viable online (-) and offline (●) and total online (-) and offline (●) cell densities. Online (-) and offline (●) viable cell percentages. (b) Online predicted infected cell fraction (-), offline measurements of fraction of GFP (●) and mCherry (●) expressing cells, and average online cell diameter (-). Error bars represent duplicate measurement values

cell count methods (data not included). This indicates that cells might be lost due to cell attachment, disintegration, or other reasons during sampling, diluting, and mixing of cell suspension samples from the bioreactor. The online measurement showed a clear peak in the viable cell density, whereas the manual counts showed a plateau in the viable cells followed by a decrease in viable cells. This demonstrated that due to the high resolution of online measurements, the exact moment where the cells stop growing could be determined. The viability estimated by the online microscope showed a similar trend as the manual value, although the offline measured values were higher towards the end of the cell culture when the viability dropped (Figure 3a). This could be due to the difference in measurement principle. The manual method is based on membrane permeability. The microscope method is based on alterations in the optical properties of the cell, which may occur before the membrane becomes permeable, thus resulting in lower viable cell percentages. Furthermore, as cells start to die, the morphology of the cell population becomes more heterogeneous. The increase in heterogeneity complicates cell measurements and can cause inaccuracies in both offline and online methods mainly due to cell clumping and decreasing cell circularity.

Based on offline flow cytometer measurements of low MOI infected cells, expression of green fluorescence was detected only slightly earlier than red fluorescence and this was well predicted by the iLine F. The start of mCherry expression was almost at the same moment as the start of eGFP expression, where it is expected to start 16–20 h later as observed previously for high MOI infections. Possibly this is due to the low resolution of offline measurements with only one measurement taken when baculovirus infection started to spread throughout the cell culture. In contrast, the iLine F was able to continuously follow the progression of baculovirus infection and predict the percentage of infected insect cells in real-time, in this case also for infections that were started at a low MOI and thus requiring multiple infection cycles to infect all the cells at 93 hpi (Figure 3b). This moment coincided with the stabilization of the total cell density as measured in real-time by the iLine F. Viable cell density peaked and the cell viability started to decrease around the same moment. Slower cell growth was observed before the first infected cells were detected between 70 and 80 hpi. This could be due to the delay between actual infection and the appearance of optical changes in the cell as discussed with the calibration experiments. In addition, it could also partly be due to the multiple infection cycles needed to infect all the cells. However, it was not possible to make a clear distinction between sequential infection cycles from the online measurements of infected cells. When infecting with an MOI of 0.01, <1% of the cells are expected to be initially infected. This is close to the detection limit of the system. Some measurement noise existed in the online signal of the fraction of infected cells, especially during the first 24 and final 10 h. During cell culture, there are typically moments where cells experience high stress due to respective inoculation, apoptotic signals, budded virus production, and cell death.[27–30] These events may influence cell morphology, such as average cell diameter, which in turn affects the infected cell prediction. Additional training with new datasets could improve the accuracy and sensitivity of the infected cell detection algorithm to reduce this measurement noise and possibly detect the different infection cycles during low MOI baculovirus infection processes.

3.3 | Online monitoring of baculovirus infection at different MOIs

Using the machine learning model calibrated on immediate early expression, ExpiSf9 cell infection was monitored for bioreactor processes where fluorescent proteins were expressed behind the very

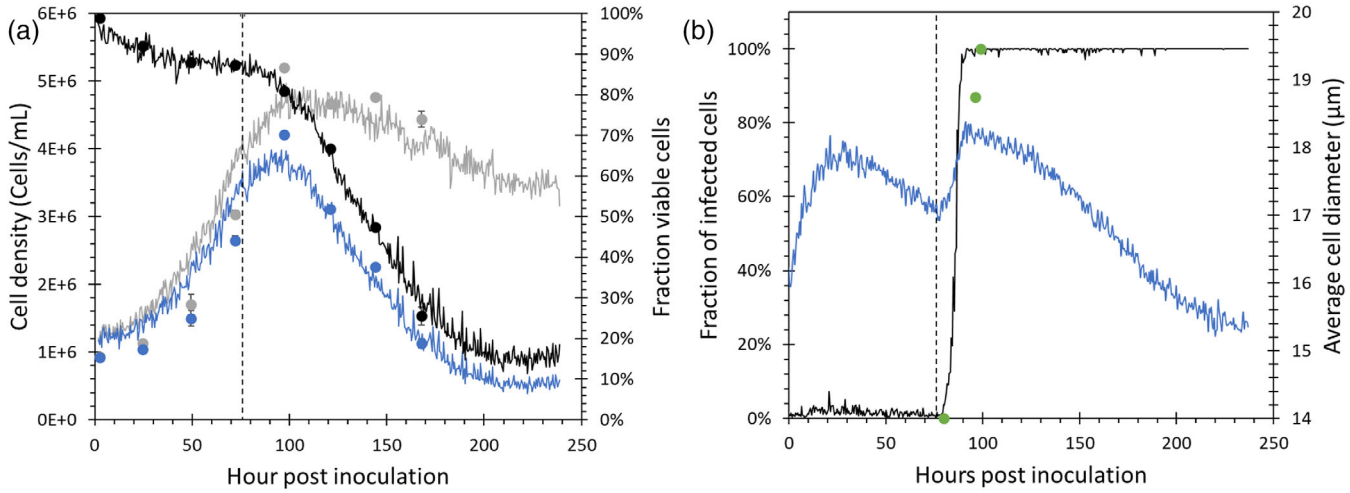

FIGURE 4 Time-course profiles of a bioreactor infected with MOI 10. ExpiSf9 cells were infected with a baculovirus expressing GFP from the very late polyhedrin promoter at an MOI of 10. The dashed lines indicate the moment of baculovirus infection. (a) Viable online (-) and offline (●) and total online (-) and offline (●) cell densities. Online (-) and offline (●) viable cell percentages. (b) Online predicted infected cell fraction (-), offline measurements of fraction of GFP expressing cells (●), and average online cell diameter (-). Error bars represent duplicate measurement values

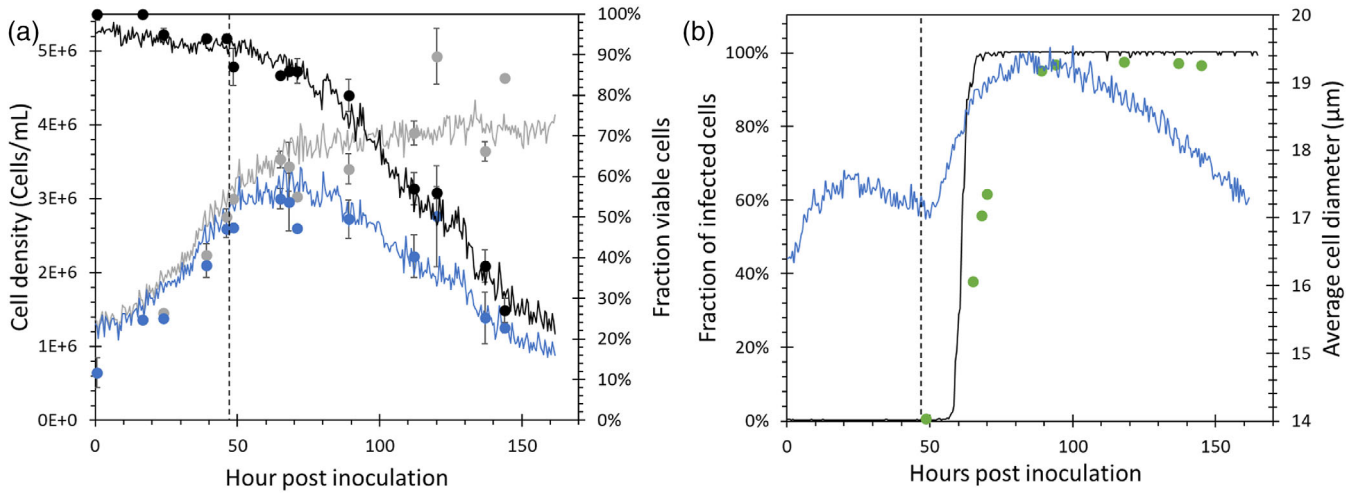

FIGURE 5 Time-course profiles of a bioreactor infected with MOI 1. ExpiSf9 cells were infected with a baculovirus expressing GFP at an MOI of 1. This baculovirus construct contained a gene for GFP located behind the very late polyhedrin promoter. The dashed lines indicate the moment of baculovirus infection. (a) Viable online (-) and offline (●) and total online (-) and offline (●) cell densities. Online (-) and offline (●) viable cell percentages. (b) Online predicted infected cell fraction (-), offline measurements of fraction of GFP expressing cells (●), and average online cell diameter (-). Error bars represent duplicate measurement values

late polyhedrin promoter, which is the strongest baculovirus promoter and most commonly exploited for the expression of recombinant proteins with the BEVS.[31,32] All bioreactor runs were monitored with the iLine F microscope to follow baculovirus infection inside the cells. MOIs between 0.01 and 10 were used to investigate differences between immediate cell infection and slower infection processes involving multiple infection cycles inside the production bioreactor.

With the iLine F, it was possible to monitor the fraction of infected cells in real time for different MOIs. For the high MOI processes, infection development was faster and 100% cell infection was reached within 9 h after infection for MOI 10 and within 17 h for MOI 1 (Figures 4b and 5b). With the iLine F, infected cells could be detected before offline detection of fluorescent cells by flow cytometry. For the lower MOI process, infection development was slower and 100% of infected cells were detected only 45 h after infection (Figure 3b). Real-time measurements of average cell diameters showed a similar pattern. Average cell diameters increased more rapidly for the process infected with a high MOI (Figures 4b and 5b).

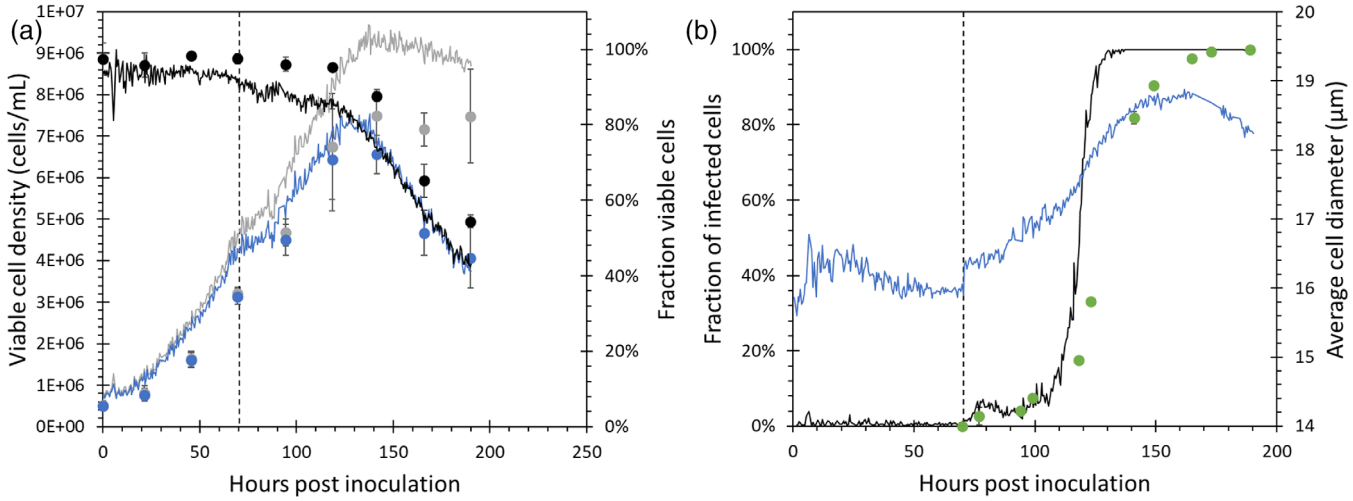

FIGURE 6 Time-course profiles of the GFP production run with butyrate addition. ExpiSf9 cells were infected with a baculovirus expressing GFP at an MOI of 0.01. This baculovirus construct contained a gene for GFP located behind the very late polyhedrin promoter. The dashed lines indicate the moment of baculovirus infection and butyrate addition. (a) Viable online (-) and offline (●) and total online (-) and offline (●) cell densities. Online (-) and offline (●) viable cell percentages. (b) Online predicted infected cell fraction (-), offline measurements of fraction of GFP expressing cells (●), and average online cell diameter (-). Error bars represent duplicate measurement values

3.4 | Verification of baculovirus-infected insect cell culture with butyrate addition

The high resolution of the online measurements ideally would allow for spotting small process deviations that might be invisible with daily manual sampling. The sensitivity of the online microscope to spot temporary effects of butyrate addition was, therefore, investigated. Butyrate was added to improve baculovirus gene expression.[18,33] ExpiSf9 cells were grown until they reached a density of 4×10^6 cells/mL at 72 hpi, at which point butyrate was added at a final concentration of 2 mM. Immediately afterward, cells were infected with an MOI of 0.01 with a baculovirus construct containing GFP behind the polyhedrin promoter. Online measurements of viable cell density and total cell density, and online predictions of cell viability and infection state were compared to offline measurements. Offline measurements of cell densities and cell viability showed a similar trend to online measurements although offline-measured cell densities were lower (Figure 6a). The online measurements showed a clear peak in the viable cell density and a sharp switch from growth to death phase, whereas the manual counts showed a plateau in the viable cells followed by a decrease in viable cells. This demonstrates once more that due to the high resolution of online measurements, the exact moment when the cells stop growing can be determined. Together with the virus, butyrate was added to the cell culture at 72 hpi to enhance GFP production. A temporary slowdown of cell growth was visible between 72 and 85 h in the high-resolution data of the online viable cell and total cell density measurement (Figure 6a). This is in agreement with the fact that butyrate can cause a cell-cycle arrest.[34] Note that this arrest is not visible in the low-resolution offline data, showing the importance of having a high-resolution online measurement. Online monitoring of the infected percentage of cells showed a small peak around 80 hpi after which the fraction of infected cells stays slightly elevated at about 5%, followed by a sharp increase around 120 hpi (Figure 6b). Such a small peak was not expected when infecting with an MOI of 0.01. It could be caused by the diameter increase of the cells directly after butyrate addition since the prediction algorithm mainly makes predictions based on the size of the cell. This indicates the potential limitation of the current model of having a strong dependency on certain parameters when using a machine learning modeling approach. Generating additional training sets specifically aimed at breaking this correlation, for instance by changing culture osmolality, could potentially improve the accuracy of the infection prediction algorithm. The small peak around 80 hpi was not clearly visible with the offline measurements GFP fluorescence at this point is unexpected as the polyhedrin promoter becomes active at 20 hpi.[26]

3.5 | Online monitoring of SARS-CoV-2 spike protein production using a low MOI

To follow the infection process for non-reporter-secreted proteins, the holographic microscope was used to monitor a SARS-CoV-2 spike protein production process (Figure 7). In contrast to reporter proteins such as GFP and mCherry, which accumulate inside the cells,[35] the S1 subunit of the SARS-CoV-2 spike protein is excreted into the medium.[9] To produce SARS-CoV-2 S1, insect cells were infected with an MOI of 0.01 at 70 hpi. S1 was detected for the first time in the culture fluid at 140 hpi and S1 concentration continued to increase until harvest at 190 hpi. Using the holographic microscope and the previously calibrated infected cell detection algorithm, the moment of 100% infected cells was detected at 155 hpi (Figure 7b). Peak viable cell density was reached a little bit earlier, at 150 hpi (Figure 7a). The

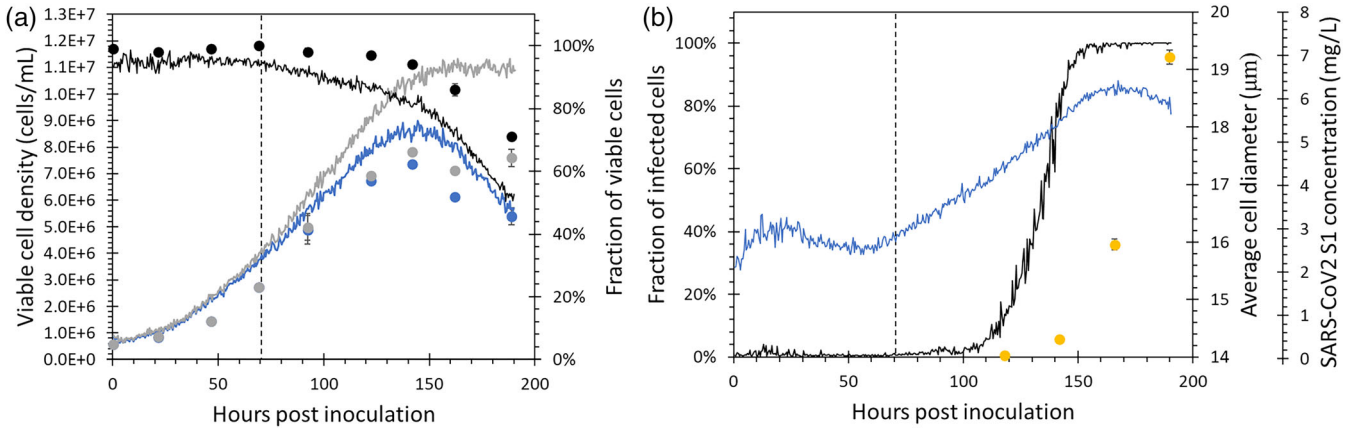

FIGURE 7 Time-course profiles of a SARS-CoV-2 S1 production run. ExpiSf9 cells were infected with a baculovirus expressing SARS-CoV-2 S1 subunits at an MOI of 0.01. The gene for expression of SARS-CoV-2 S1 was located behind the very late polyhedrin promoter. The dashed lines indicate the moment of baculovirus infection and butyrate addition. (a) Viable online (-) and offline (●) and total online (-) and offline (●) cell densities. Online (-) and offline (●) viable cell percentages. (b) Online predicted infected cell fraction (-), average online cell diameter (-), and offline measured SARS-CoV2 S1 concentrations (●). Error bars represent duplicate measurement values

reactor content was harvested when cell viability dropped below 70%. Again, the cell densities measured by the iLine F were slightly higher and the viability slightly lower than the offline samples. For the percentage of infected cells, a small increase could be observed at about 10 h after infection (80 hpi), which might represent the start of the second infection cycle. Next, the infection increased to 100% between 100 and 150 hpi (30–80 h after infection) for a low MOI process. About 30 h after the infection percentage started to rise, at 118 hpi, the secretion of the spike protein started, which is within the range expected for very late gene expression.[24]

The ideal TOH depends on product concentration and product quality. Since both parameters are relatively difficult to measure in real-time, the online measured viability, diameter, and percentage of infected cells can be used as indicators for determining the best moment of harvest. Low viability can affect protein quality, as proteases are released from dead cells.[36,37] Harvesting too early, however, can negatively affect product yield. Sander et al.[38] already demonstrated that peak protein production was reached 1 or 2 days after the point of maximum average cell diameter, showing diameter to be a good indicator for determining optimal harvest time in terms of peak protein yield. The combination of a real-time percentage of infected cells, average cell diameter, and cell viability can present a clearer picture of the state of the cell culture to determine the optimal moment of harvest. As all these parameters are measured in real-time, trends can be spotted faster and bioreactor harvest can commence instantaneously once the desired parameter criteria are met. This removes the need for offline sampling, reducing delays and inaccuracies associated with offline sample handling. Furthermore, monitoring the progress of infection is crucial to spot process deviations early on and determine the exact moment when all cells have been infected. In case of a delay, process deviations are spotted later by offline measurements, and the timings of process decisions are sub-optimal. For low MOI processes, this delay affects robustness and reproducibility to a greater extent. Since several infection cycles are necessary to reach 100% infected cells, the time to reach 100% infection can be significantly influenced by relatively small deviations at the moment of infection, for example in the titer of the baculovirus stock and amount of virus stock added. This makes low MOI processes generally less predictable. Being able to consistently execute low MOI processes with high reproducibility is highly advantageous from a process development point of view. Small virus stocks can be used, avoiding the need for a separate large-scale virus production run and subsequent virus titer determination. This leads to considerable time savings at the industrial production scale.[39] Such time savings are of utmost importance to speed up process development, especially when a rapid response to pandemic outbreaks, such as the recent SARS-CoV-2 outbreak, is needed. This study shows that with a limited training set (limited number of process conditions and virus constructs) the microscope and machine learning algorithm can predict cell numbers, viability, and infection percentage for different viral constructs, MOIs, and butyrate addition. However, the model heavily relies on the increase in cell size for predicting the infected cell percentage. This could be a limitation in case process conditions are introduced that cause changes in cell size. Further training of the model using such conditions could further improve the accuracy and applicability of the model. The high resolution of the online measurements enables the detection of small events or process deviations that would have otherwise been missed by manual sampling. Detecting these deviations gives more insight into the state of the culture and could aid in process understanding and process control.

4 | CONCLUSION

Online double differential digital holographic microscopy (D3HM) and machine learning modeling was used for real-time monitoring of insect cell proliferation and baculovirus infection in bioreactors. Training and verification data sets were generated using a purpose-built

baculovirus construct. Calibration of the machine learning model was based on infection with a baculovirus that had eGFP behind an early promotor. With the online microscope, it was possible to accurately monitor viable and total cell densities, viable cell percentages, and insect cell infection states for a variety of baculovirus constructs, MOIs, and produced proteins based on this calibration data set. Moreover, the high resolution of the online measurements made it possible to accurately determine changes in the culture like the exact moment of peak cell densities and detection of growth arrest due to butyrate addition. Accurate online monitoring of bioreactor cell cultures with high resolution is important to enhance process understanding and may aid in the timing of important process steps such as the time of infection or the time of harvest. Each newly generated data set can be used to improve the machine learning algorithms and can be used retroactively by re-calculating old data sets. The variety of cell parameters computed by the microscope potentially hides a wealth of information on the biological state of the cells. Interpreting this information to obtain further insight into the state of the cell culture, and in real-time, is a future challenge.

AUTHOR CONTRIBUTIONS

Jort J. Altenburg: Conceptualization (equal); data curation (equal); formal analysis (equal); investigation (equal); methodology (equal); project administration (equal); resources (equal); software (equal); supervision (equal); validation (equal); visualization (lead); writing – original draft (lead). **Maarten Klaverdijk:** Investigation (equal); writing – review and editing (equal). **Damien Cabosart:** Data curation (equal); methodology (equal); writing – review and editing (equal). **Laurent Desmecht:** Data curation (equal); methodology (equal). **Sonja S. Brunekreeft-Terlouw:** Investigation (equal); writing – review and editing (equal). **Joshua Both:** Investigation (equal); writing – review and editing (equal). **Vivian I. P. Tegelbeckers:** Investigation (equal); writing – review and editing (equal). **Marieke L. P. M. Willekens:** Investigation (equal); writing – review and editing (equal). **Linda van Oosten:** Investigation (equal); resources (equal); writing – review and editing (equal). **Tessy A. H. Hick:** Investigation (equal); writing – review and editing (equal). **Tom M. H. van der Aalst:** Investigation (equal); writing – review and editing (equal). **Gorben P. Pijlman:** Funding acquisition (equal); supervision (equal); writing – review and editing (equal). **Monique M. van Oers:** Funding acquisition (lead); resources (equal); supervision (equal); writing – review and editing (equal). **René H. Wijffels:** Funding acquisition (equal); project administration (equal); resources (equal); supervision (equal); writing – review and editing (equal). **Dirk E. Martens:** Conceptualization (equal); funding acquisition (equal); project administration (equal); resources (equal); supervision (equal); writing – review and editing (equal).

ACKNOWLEDGMENTS

We thank Els Roode, Gwen Nowee, Fred van den End, and Wendy Evers (Wageningen University & Research) for their technical assistance. We also acknowledge Jérémie Baurbau, Jan van Hauwermeieren, Nicolas Janssen, Willem Hoerée, and Thomas Guyon (Ovizio) for their assistance and advice in using the iLine F. We thank Tom van Arragon and Timo Keijzer (Getinge) for their bioreactor support. This publication is part of the BACFREE project with project number 16762 of the Open Technology Programme, which is (partly) financed by the Dutch Research Council (NWO). Damien Cabosart and Laurent Desmecht are employees of Ovizio.

PEER REVIEW

The peer review history for this article is available at https://publons.com/publon/10.1002/btpr.3318.

DATA AVAILABILITY STATEMENT

Data available on request from the authors.

ORCID

Jort J. Altenburg https://orcid.org/0000-0002-9292-5339
Dirk E. Martens https://orcid.org/0000-0002-5662-0466

REFERENCES

1. Luckow VA, Summers MD. Trends in the development of baculovirus expression vectors. *BioTechnology*. 1988;6(1):47-55. doi:10.1038/nbt0188-47
2. Possee RD. Baculoviruses as gene expression vectors. *Annu Rev Microbiol*. 1988;42:177-199. doi:10.1146/annurev.mi.42.100188.001141
3. Kost T. Recombinant baculoviruses as expression vectors for insect and mammalian cells. *Curr Opin Biotechnol*. 1999;10(5):428-433. doi:10.1016/S0958-1669(99)00005-1
4. Pijlman GP. Enveloped virus-like particles as vaccines against pathogenic arboviruses. *Biotechnol J*. 2015;10(5):659-670. doi:10.1002/biot.201400427
5. van Oers MM. Opportunities and challenges for the baculovirus expression system. *J Invertebr Pathol*. 2011;107(Suppl):S3-S15. doi:10.1016/j.jip.2011.05.001
6. Kost TA, Condreay JP, Jarvis DL. Baculovirus as versatile vectors for protein expression in insect and mammalian cells. *Nat Biotechnol*. 2005;23(5):567-575. doi:10.1038/nbt1095
7. Roldão A, Mellado MCM, Castilho LR, Carrondo MJT, Alves PM. Virus-like particles in vaccine development. *Expert Rev Vaccines*. 2010;9(10):1149-1176. doi:10.1586/erv.10.115
8. Cox M. Modern technology: the preferred biosecurity strategy? *Vaccine*. 2017;35(44):5949-5950. doi:10.1016/j.vaccine.2017.03.048
9. van Oosten L, Altenburg JJ, Fougeroux C, et al. Two-component nanoparticle vaccine displaying glycosylated spike S1 domain induces neutralizing antibody response against SARS-CoV-2 variants. *MBio*. 2021;12:e0181321. doi:10.1128/mbio.01813-21
10. Shinde V, Bhikha S, Hoosain Z, et al. Efficacy of NVX-CoV2373 Covid-19 vaccine against the B.1.351 variant. *N Engl J Med*. 2021;384(20):1899-1909. doi:10.1056/nejmoa2103055
11. Anurag SR, Winkle H. Quality-by-design approach. *Nat Biotechnol*. 2009;27(1):26-34. doi:10.1038/nbt0109-26
12. Kiviharju K, Salonen K, Moilanen U, Meskanen E, Leisola M, Eerikäinen T. On-line biomass measurements in bioreactor cultivations: comparison study of two on-line probes. *J Ind Microbiol Biotechnol*. 2007;34(8):561-566. doi:10.1007/s10295-007-0233-5
13. Carvell JP, Dowd JE. On-line measurements and control of viable cell density in cell culture manufacturing processes using radio-frequency impedance. *Cytotechnology*. 2006;50(1–3):35-48. doi:10.1007/s10616-005-3974-x
14. Ude C, Schmidt-Hager J, Findeis M, John GT, Scheper T, Beutel S. Application of an online-biomass sensor in an optical multisensory platform prototype for growth monitoring of biotechnical relevant

microorganism and cell lines in single-use shake flasks. *Sensors*. 2014;14(9):17390-17405. doi:10.3390/s140917390
15. Rappaz B, Breton B, Shaffer E, Turcatti G. Digital holographic microscopy: a quantitative label-free microscopy technique for phenotypic screening. *Comb Chem High Throughput Screen*. 2014;17(1):80-88. doi:10.2174/13862073113166660062
16. Janicke B, Kårsnäs A, Egelberg P, Alm K. Label-free high temporal resolution assessment of cell proliferation using digital holographic microscopy. *Cytom Part A*. 2017;91(5):460-469. doi:10.1002/cyto.a.23108
17. Pais DAM, Galrão PRS, Kryzhanska A, Barbau J, Isidro IA, Alves PM. Holographic imaging of insect cell cultures: online non-invasive monitoring of adeno-associated virus production and cell concentration. *Processes*. 2020;8(4). doi:10.3390/PR8040487
18. Yovcheva M, Thompson K, Barnes S, et al. High-titer recombinant protein production. *Genet Eng Biotechnol News*. 2018;38(13):20-21. doi:10.1089/gen.38.13.08
19. Hopkins RF, Esposito D. A rapid method for titrating baculovirus stocks using the sf-9 easy titer cell line. *Biotechniques*. 2009;47(3):785-788. doi:10.2144/000113238
20. Schopf B, Howaldt MW, Bailey JE. DNA distribution and respiratory activity of *Spodoptera frugiperda* populations infected with wild-type and recombinant *Autographa californica* nuclear polyhedrosis virus. *J Biotechnol*. 1990;15(1–2):169-185. doi:10.1016/0168-1656(90)90059-K
21. Kamen AA, Bédard C, Tom R, Perret S, Jardin B. On-line monitoring of respiration in recombinant-baculovirus infected and uninfected insect cell bioreactor cultures. *Biotechnol Bioeng*. 1996;50(1):36-48. doi:10.1002/(SICI)1097-0290(19960405)50:13.0.CO;2-2
22. Taticek RA, Shuler ML. Effect of elevated oxygen and glutamine levels on foreign protein production at high cell densities using the insect cell-baculovirus expression system. *Biotechnol Bioeng*. 1997;54(2):142-152. doi:10.1002/(SICI)1097-0290(19970420)54:23.0.CO;2-L
23. Palomares LA, Pedroza JC, Ramírez OT. Cell size as a tool to predict the production of recombinant protein by the insect-cell baculovirus expression system. *Biotechnol Lett*. 2001;23(5):359-364. doi:10.1023/A:1005688417525
24. Ramachandran A, Bashyam MD, Viswanathan P, Ghosh S, Kumar MS, Hasnain SE. The bountiful and baffling baculovirus: the story of polyhedrin transcription. *Curr Sci*. 2001;81(8):998-1010.
25. Shippam-Brett CE, Willis LG, Theilmann DA. Analysis of sequences involved in IE2 transactivation of a baculovirus immediate-early gene promoter and identification of a new regulatory motif. *Virus Res*. 2001;75(1):13-28. doi:10.1016/S0168-1702(00)00253-7
26. Massotte D. G protein-coupled receptor overexpression with the baculovirus-insect cell system: a tool for structural and functional studies. *Biochim Biophys Acta – Biomembr*. 2003;1610(1):77-89. doi:10.1016/S0005-2736(02)00720-4
27. Kiehl TR, Shen D, Khattak SF, Jian Li Z, Sharfstein ST. Observations of cell size dynamics under osmotic stress. *Cytom Part A*. 2011;79 A(7):560-569. doi:10.1002/cyto.a.21076
28. Byun S, Hecht VC, Manalis SR. Article characterizing cellular biophysical responses to stress by relating. *Biophys J*. 2015;109(8):1565-1573. doi:10.1016/j.bpj.2015.08.038
29. Huang N, Wu W, Yang K, Passarelli AL, Rohrmann GF, Clem RJ. Baculovirus infection induces a DNA damage response that is required for efficient viral replication. *J Virol*. 2011;85(23):12547-12556. doi:10.1128/jvi.05766-11
30. Weidner T, Druzinec D, Mühlmann M, Buchholz R, Czermak P. The components of shear stress affecting insect cells used with the baculovirus expression vector system. *Zeitschrift Fur Naturforsch – Sect C J Biosci*. 2017;72(9–10):429-439. doi:10.1515/znc-2017-0066
31. Smith GE, Fraser MJ, Summers MD. Molecular engineering of the *Autographa californica* nuclear polyhedrosis virus genome: deletion mutations within the polyhedrin gene. *J Virol*. 1983;46(2):584-593. doi:10.1128/jvi.46.2.584-593.1983
32. Van Oers MM, Pijlman GP, Vlak JM. Thirty years of baculovirus-insect cell protein expression: from dark horse to mainstream technology. *J Gen Virol*. 2015;96(1):6-23. doi:10.1099/vir.0.067108-0
33. Guo R, Zhang Y, Liang S, Xu H, Zhang M, Li B. Sodium butyrate enhances the expression of baculovirus-mediated sodium/iodide symporter gene in A549 lung adenocarcinoma cells. *Nucl Med Commun*. 2010;31(10):916-921. doi:10.1097/MNM.0b013e32833dedd7
34. Peng Y, Song J, Lu J, Chen X. The histone deacetylase inhibitor sodium butyrate inhibits baculovirus-mediated transgene expression in Sf9 cells. *J Biotechnol*. 2007;131(2):180-187. doi:10.1016/j.jbiotec.2007.06.009
35. Oker-Blom C, Orellana A, Keinanen K. Highly efficient production of GFP and its derivatives in insect cells for visual in vitro applications. *FEBS Lett*. 1996;389(3):238-243. doi:10.1016/0014-5793(96)00593-5
36. Pyle LE, Barton P, Fujiwara Y, Mitchell A, Fidge N. Secretion of biologically active human proapolipoprotein A-I in a baculovirus-insect cell system: protection from degradation by protease inhibitors. *J Lipid Res*. 1995;36(11):2355-2361. doi:10.1016/s0022-2275(20)39716-9
37. Heitz F, Nay C, Guenet C. Expression of functional human muscarinic M2 receptors in different insect cell lines. *J Recept Signal Transduct Res*. 1997;17(1–3):305-317. doi:10.3109/10799899709036611
38. Sander L, Harrysson ÆA. Using cell size kinetics to determine optimal harvest time for *Spodoptera frugiperda* and *Trichoplusia ni* BTI-TN-5B1-4 cells infected with a baculovirus expression vector system expressing enhanced green fluorescent protein. *Cytotechnology*. 2007;54:35-48. doi:10.1007/s10616-007-9064-5
39. Maranga L, Brazao TF, Carrondo MJT. Virus-like particle production at low multiplicities of infection with the baculovirus insect cell system. *Biotechnol Bioeng*. 2003;84(2):245-253. doi:10.1002/bit.10773

How to cite this article: Altenburg JJ, Klaverdijk M, Cabosart D, et al. Real-time online monitoring of insect cell proliferation and baculovirus infection using digital differential holographic microscopy and machine learning. *Biotechnol. Prog*. 2022;e3318. doi:10.1002/btpr.3318